Phase Transitions

International Edition: DOI: 10.1002/anie.201803176
German Edition: DOI: 10.1002/ange.201803176

An Unusual Phase Transition Driven by Vibrational Entropy Changes in a Hybrid Organic–Inorganic Perovskite

Wenjuan Wei, Wei Li, Keith T. Butler,* Guoqiang Feng, Christopher J. Howard, Michael A. Carpenter,* Peixiang Lu,* Aron Walsh, and Anthony K. Cheetham*

Abstract: *The driving forces for the phase transitions of ABX_3 hybrid organic–inorganic perovskites have been limited to the octahedral tilting, order–disorder, and displacement. Now, a complex structural phase transition has been explored in a HOIP, $[CH_3NH_3][Mn(N_3)_3]$, based on structural characterizations and ab initio lattice dynamics calculations. This unusual first-order phase transition between two ordered phases at about 265 K is primarily driven by changes in the collective atomic vibrations of the whole lattice, along with concurrent molecular displacements and an unusual octahedral tilting. A significant entropy difference ($4.35\ J\,K^{-1}\,mol^{-1}$) is observed between the low- and high-temperature structures induced by such atomic vibrations, which plays a main role in driving the transition. This finding offers an alternative pathway for designing new ferroic phase transitions and related physical properties in HOIPs and other hybrid crystals.*

Hybrid organic–inorganic perovskites (HOIPs) have attracted growing interest in recent years owing to their potential applications in the fields of photovoltaics, optoelectronics, and sensing devices.[1] Similar to their conventional oxide counterparts, HOIPs exhibit abundant structural transitions in response to external perturbation.[2–4] Since these phase transitions (PTs) often lead to significant changes in the electrical, magnetic, and optical properties that are of vital importance for the design and fabrication of functional devices,[5,6] it is crucial to fully understand their origins at the atomic scale.

In traditional inorganic perovskites, displacements and octahedral tilting are the primary driving forces for PTs.[7,8] However, the presence of organic species on the A and/or X sites in HOIPs significantly complicates the symmetry breaking process.[2,9,10] Although octahedral tilting patterns in HOIPs are generally reminiscent of those in conventional perovskites, their larger and longer X-site linkers offer additional freedom for the octahedra to distort, hence offering new tilting possibilities.[11–13] On the other hand, the dynamic movement of the organic A site from one state to another, which normally appears as order–disorder switching via rotational and configurational changes, can also induce symmetry changes.[14–17] The accompanying alterations of hydrogen bonding[18] and dispersive forces[19] during the dynamic switching will in turn influence the PT. Such complex synergies in the A site have been found to be the main origin of ferroelectricity in some HOIPs,[20] in stark contrast to the displacive nature of electrical ordering in perovskite oxides.[21,22]

Although the importance of PTs in HOIPs has attracted increasing awareness, most studies have focused on the aforementioned driving factors of octahedral tilting, molecular ordering and displacement.[2] Two prominent differences between HOIPs and inorganic perovskites are their lower formula weights and much more flexible X-sites, which can lead to energetic changes across a transition associated with vibrational entropy effects. Such vibrational entropy effects have been found to be the primary factor for driving polymorphism in hybrid formates according to recent lattice dynamics calculations.[23] Herein we report an unusual vibrational entropy change-driven PT in an azide HOIP, $[CH_3NH_3][Mn(N_3)_3]$, on the basis of comprehensive structural and thermodynamic characterisations, as well as detailed lattice dynamics calculations. We show that the complex first-order PT in $[CH_3NH_3][Mn(N_3)_3]$ involves the synergistic motions of the octahedral tilting, rotation and displacement of the $CH_3NH_3^+$ cation, and motion of the azide group. As a result, we find that a significant entropy change across the transition arising primarily from atomic vibrations of the lattice plays a central role in its mechanism.

[*] W. Wei, Prof. W. Li, Dr. G. Feng, Prof. P. Lu
School of Physics, Huazhong University of Science and Technology
Wuhan 430074 (China)
E-mail: wl276@hust.edu.cn
lupeixiang@hust.edu.cn

Dr. K. T. Butler
ISIS Facility, Rutherford Appleton Laboratory, Harwell Oxford
Didcot, Oxfordshire OX11 0QX (UK)
E-mail: keith.butler@stfc.ac.uk

Prof. C. J. Howard
School of Engineering, University of Newcastle
New South Wales 2308 (Australia)

Prof. M. A. Carpenter
Department of Earth Sciences, University of Cambridge
Cambridge, CB2 3EQ (UK)
E-mail: mc43@esc.cam.ac.uk

Prof. P. Lu
Laboratory of Optical Information Technology
Wuhan Institute of Technology
Wuhan 430205 (China)

Prof. A. Walsh
Department of Materials
Imperial College London, Royal School of Mines
London SW7 2AZ (UK)

Prof. A. K. Cheetham
Department of Materials Science and Metallurgy
University of Cambridge
Cambridge CB3 0FS (UK)

Supporting information and the ORCID identification number(s) for the author(s) of this article can be found under: https://doi.org/10.1002/anie.201803176.

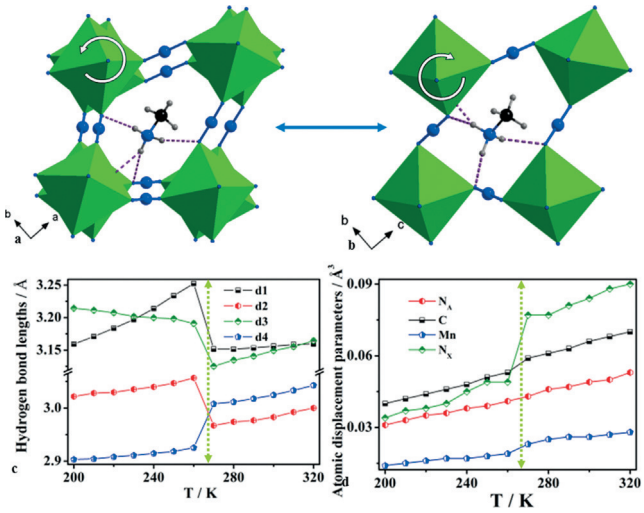

Figure 1. a),b) Crystal structures of the HT (270 K) and LT (260 K) phases viewed down the *c* and *a* axis, respectively. Violet dotted lines signify the hydrogen bonds. The gray arrows indicate the rotation directions of octahedra during the PT. Mn green, C black, N blue, H gray. c) N–H···N hydrogen bond distances as a function of temperature. d) Temperature dependence of ADPs of Mn, C, N_A, and N_X atoms. N_A and N_X represent the nitrogen atoms of the A and X sites, respectively; the green vertical line separates the LT and HT phase regions.

$[CH_3NH_3][Mn(N_3)_3]$ has an ABX_3 perovskite structure in which the A, B, and X sites are $CH_3NH_3^+$, Mn^{2+}, and azide groups, respectively. The high-temperature (HT) structure (270 K, Figure 1a) of $[CH_3NH_3][Mn(N_3)_3]$ crystallizes in the monoclinic space group $P2_1/c$, with $a = 9.0311(10)$, $b = 7.3935(8)$, $c = 12.5463(13)$ Å, $\beta = 102.434(11)°$ and $V = 818.09(16)$ Å^3, in which the fully ordered $CH_3NH_3^+$ is hydrogen-bonded to the $[Mn(N_3)_3]^-$ perovskite framework.[24] There are four hydrogen bonds in each pseudo-perovskite unit and the N···N distances and N–H···N angles are 2.967(3)–3.152(4) Å and 130.0(5)–171.4(4)°, respectively. Notably, the $CH_3NH_3^+$ cation is located in the perovskite cavity at an off-centre position along the *c* axis and the adjacent MnN_6 octahedra distort along this direction. According to the Glazer notation, the octahedral tilting system of the HT phase would be $a^-b^-b^-$.[25] The HT $P2_1/c$ structure has cell dimensions of about $\sqrt{2}a_c \times \sqrt{2}a_c \times 2a_c$ with reference to a notional perovskite-like cubic parent structure with space group $Pm\bar{3}m$ and cell parameter a_c.

Upon cooling, $[CH_3NH_3][Mn(N_3)_3]$ undergoes a PT at about 265 K to a low temperature (LT) phase with the same monoclinic space group $P2_1/c$, but with $a = 6.2218(4)$, $b = 7.2500(4)$, $c = 18.3398(11)$ Å, $\beta = 102.075(5)°$, and $V = 808.97(8)$ Å^3 (Figure 1b).[24] With respect to the same parent cubic structure, the cell dimensions of the LT structure are about $a_c \times \sqrt{2}a_c \times 2\sqrt{2}a_c$. This structure does not have a group-subgroup relationship with the HT structure, so the transition must be first-order in character, with a complex pattern of changes which involves all the A, B, and X sites. Specifically, on passing through the PT the $CH_3NH_3^+$ cation exhibits both displacement and rotation about the C–N axis, and the MnN_6 octahedral tilts change dramatically (the Glazer notation is no longer applicable) along with significant movement of the azide groups. This is accompanied by the breaking and reforming of hydrogen bonding, giving rise to N···N distances of 2.925(2)–3.252(3) Å and N–H···N angles of 149.2(3)–158.6(3)° (Figure 1b). Strikingly, three reconstructed hydrogen bonds in the LT structure are about 2.1–3.2% longer than those in the HT structure, though the fourth one is slightly shorter (ca. 2.8%; Figure 1c). This results in overall weakening of the hydrogen-bonding when crossing the transition from HT to LT, which has not been reported in any other HOIPs.[2] However, the thermal vibrations of all atoms in $[CH_3NH_3][Mn(N_3)_3]$ show a normal trend, where the atomic displacement parameters (ADPs) of C, N_A, Mn, and N_X all decrease upon cooling (Figure 1d), though there is a sharp drop in the ADPs of the azide nitrogen atoms. This unusual phenomenon arises from the competing effects of electrostatic interactions and hydrogen bonding in the perovskite unit across the transition. The unit cell volume contracts by about 1.13% when cooling from 270 to 260 K, leading to a significant increase of electrostatic interactions between the $CH_3NH_3^+$ cation and the perovskite host, which compensates for the lengthening of the hydrogen bonding and results in overall decreasing ADPs from HT to LT. Further resonant ultrasound spectroscopy experiments indicate the relaxations of hydrogen bonding across the transition could happen at a time scale of about 10^{-5}–10^{-6} s[26,27] and the associated significant energy loss spanning about 100 K is fundamentally different from those order–disorder scenarios in other HOIPs (Supporting Information, Figure S3).[28,29]

Differential scanning calorimetry plots show sharp peaks at 277 K on heating and at 264 K on cooling which confirms the strong first-order nature of the transition (Supporting Information, Figure S4a).[24] The temperature dependencies of the entropy (S_{Exp}), shown in the Supporting Information, Figure S4b, demonstrate that the associated entropy change (ΔS_{Exp}) is about 4.35 J K^{-1} mol^{-1}. This rather large value is close to that of a two-fold order-disorder transition ($\Delta S = R\ln N_2/N_1 = R\ln 2 = 5.76$ J K^{-1} mol^{-1}, where N_2/N_1 represents the ratio of possible configurations after and before PT and R is the gas constant), though our single-crystal X-ray diffraction studies exclude the existence of any obvious structural disorder in the HT phase. Such an unusually large entropy change suggests that the structure exhibits a significant increase in the vibrational degrees of freedom and corresponding active phonon modes on transitioning from the LT to HT structure.

To better understand the distortions in these structures, the $[Mn(N_3)_3]^-$ frameworks have been compared with the framework of a notional cubic parent framework in space group $Pm\bar{3}m$ (Supporting Information, Figure S5),[30] using the computer program ISODISTORT.[31] A very significant distortion in each structure is associated with irreducible representation (irrep) M_3^- (at $k = {}^1/_2,{}^1/_2,0$); this distortion has been described elsewhere as a "columnar shift".[9] In the HT structure there is also significant distortion associated with irrep R_4^+, which is well known in perovskites to give out-of-phase octahedral tilting and in this case the tilt system $a^-b^-b^-$. In the LT structure, there is no contribution from R_4^+, but rather a significant contribution from peculiar irrep Σ_2 (at $k =$

$^1/_4,^1/_4,0$), which gives a pattern of tilting such that pairs of neighbouring octahedra tilt in the same sense (Supporting Information, Figure S1b). Although other distortions are present, it is sufficient to couple M_3^- with R_4^+, and M_3^- with Σ_2, to give the HT and LT structures, respectively.[32] From the perspective of the framework, the HT to LT transition may be seen largely as a change from a conventional $a^-b^-b^-$ tilt system to the unusual Σ_2 tilt system against the background of notional cubic framework distorted by irrep M_3^-. Although the changes in the framework may be interesting, it is likely that these changes are driven by changes in the orientations and locations of the $CH_3NH_3^+$ entities in the cavities. Both HT and LT structures are ferroelastic with respect to the parent cubic structure, and the HT phase does indeed contain ferroelastic twin walls at room temperature (Supporting Information, Figure S6). Even though there is no group–subgroup relationship between the HT and LT phases, it is likely that the latter will also contain abundant ferroelastic twin walls.

To fully understand the PT mechanism and origin of the associated large entropy change, we have applied lattice dynamics calculations to probe the driving forces (Supporting Information, Figures S7–S9).[33,34] The Gibbs free energy (G) is calculated by applying the quasi-harmonic approximation methodology from Equation (1):

$$G = U + F_{ph} \tag{1}$$

The internal energy of the system (U) can be obtained from density functional theory (DFT) calculations. The phonon free energy (F_{ph}) arising from harmonic vibrations of the lattice is calculated using the frozen phonon approximation according to Equation (2):

$$F_{ph} = E_{Vib} - TS_{Vib} \tag{2}$$

where E_{Vib} and S_{Vib} denote the vibrational energy and vibrational entropy of phonons, respectively. The magnetic contribution would have little effect on the calculations and has not been taken into account. The S_{Vib} is calculated from the phonon density of states (DOS) of all positive phonon modes according to Equation (3):[34]

$$S_{Vib}(T) = 3k_B \int_0^\infty g(\varepsilon)\{[n(\varepsilon)+1]\ln[n(\varepsilon)+1] - n(\varepsilon)\ln[n(\varepsilon)]\}\,d\varepsilon \tag{3}$$

where k_B is the Boltzmann constant, $g(\varepsilon)$ is the normalized phonon DOS with energy $\varepsilon = \hbar\omega$ (ω is mode frequency), and $n(\varepsilon)$ is Bose–Einstein population of a state of energy ε at temperature T.

The contributions of the phonon modes to S_{Vib} of the two phases are shown in Figure S10, which demonstrates that the HT structure exhibits larger vibrational effects at almost all phonon energies. Furthermore, the left axis in Figure 2 shows G of the HT and LT phases as a function of temperature. The internal energy difference (ΔU) between the two phases is essentially constant with varying temperature, therefore it cannot account for the crossover of the phase stability. The lack of any discontinuity in configurational entropy across the

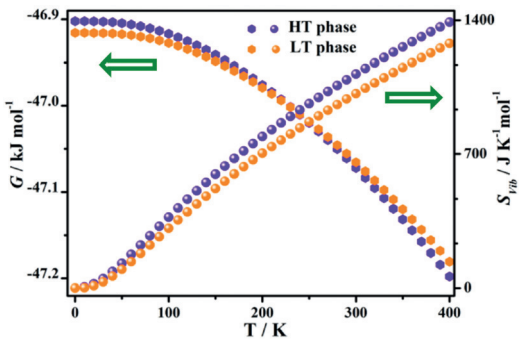

Figure 2. The vibrational entropy (S_{Vib}) and Gibbs free energy (G) for the HT and LT phases calculated from 0 to 400 K.

transition distinguishes this system from the scenarios in other HOIPs,[35,36] where dynamic configurational ordering is the main contributor to the difference in entropy between competing phases. Furthermore, the right axis of Figure 2 shows that the S_{Vib} of the HT phase is greater than that of the LT structure. As the temperature increases, the TS_{Vib} contribution to G becomes more pronounced and eventually the HT phase becomes thermodynamically more favourable than the LT phase at about 220 K, which is in reasonable agreement with the experimental value of about 265 K. At the transition temperature we obtain a value of ΔS_{Vib} of 22.75 $J K^{-1} mol^{-1}$ from the calculations, which is greater than the measured value (4.35 $J K^{-1} mol^{-1}$), the difference is most likely due to the fact that the harmonic approximation applied here does not account for the change in volume with temperature of the phases.

We also investigate which phonon modes are responsible for the difference in TS_{Vib} between the two phases. The frequency dependencies of TS_{Vib} and the integrated vibrational entropies (TS_{Tot}) of the HT and LT structures are plotted in Figures S11a and b, respectively. These plots show how the vibrational modes contribute to the entropy, depending on their frequency. The vast majority of the contribution to TS_{Vib} comes from vibrational modes with frequencies below 10 THz, which leads TS_{Tot} to reach a plateau at around 10 THz at any given temperature, indicating the domination of soft phonon modes in the lattice vibrations.

To further probe the atomistic origins of the above results, we have decomposed the fractional contribution of each structural site (A, B, and X sites) to the TS_{Tot} within the corresponding entropy range by calculating the weighted average of the phonon DOS of a given site i at energy ε, $\langle g_i(\varepsilon)\rangle = \Sigma_j \omega_{ij}/\Sigma_k \omega_k$, where ω_{ij} are the weights of the phonon modes involving the site i at energy ε, and k is the list of all sites (Figures 3 a,c).[23] The frequency dependencies of the decomposed DOS of each atom for HT and LT are plotted in Figures 3 b,d, which shows the contributions to the phonon spectrum broken down by atomic site. As seen from this, the modes that contribute most to the entropy (those below 10 THz) involve contributions from all A, B, and X sites. This confirms that these phonons are collective modes, which depend on the interactions among all sites in the structure. The collective motions determine the entropy and in turn

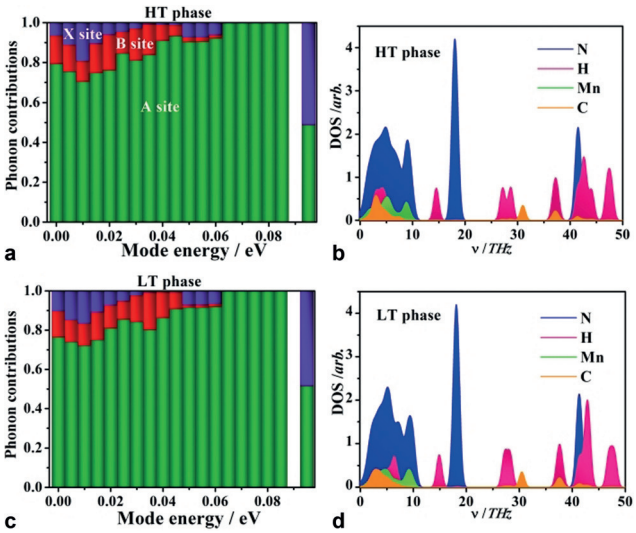

Figure 3. a),c) The fractional contribution of the A site (green), B site (red), and X site (purple) to the total vibrational entropy for a) HT and c) LT phase within the 0–0.10 eV energy range. b),d) The frequency dependencies of decomposed DOS of each atom at the b) HT and d) LT phase.

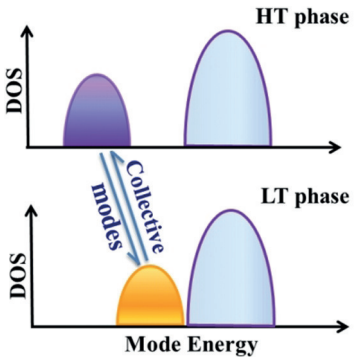

Figure 4. The physical model of the DOS as a function of the mode energy for the HT (top) and LT (bottom) phases influenced by the collective vibrational modes during PT. The lower energy branch of the DOS are the collective modes, which involve simultaneous vibration of all sites in the material; the higher energy branch of the DOS is made of localized modes, which are specific to the different sites.

depend on the strength of the interactions between the A-site molecule and the perovskite framework.

Based on these findings, we can propose a simple physical model for the forces that drive the PT. In Figure 4, we show a representation of the HOIP in its two different phases where the lower collective and higher localized energy branches are, respectively, simplified to small and large features (the full presentation of the complex changes in both phonon DOS and energy is shown in Figure 3 and the Supporting Information, Figure S11, respectively). The top phase is the HT phase, which has higher *U*. The phonon DOS are represented for both phases in the high and low panels, respectively, where the collective modes of the "softer" HT phase have lower frequencies than those of the LT phase. At low temperatures the *U* contribution dominates *G* and the LT phase is more stable. However, the collective vibrational modes become more populated (Boltzmann distribution) with increasing temperature, and the collective modes of the HT phase fill up more rapidly than those of the LT phase so that the vibrational entropy of HT increases at a faster rate. Eventually the balance of free energy between the two phases is reversed as TS_{Vib} becomes greater than ΔU. This mechanism highlights the important role of collective modes and the delicate balance of inter atomic forces in determining phase stability through accumulative atomic vibrations in certain hybrid materials. It is worth underlining that these kinds of transitions are significantly different from the widely reported order–disorder transitions which feature large entropy changes owing to configurational alterations.

In conclusion, we have comprehensively investigated the first-order phase transition in a HOIP, $[CH_3NH_3][Mn(N_3)_3]$, by a combined approach of experiments and lattice dynamics calculations. The transition is between two different subgroup structures of the notional cubic parent and is representative of the diversity of structures, properties and PTs which is emerging from this new class of HOIPs in comparison with conventional oxide perovskites. In particular, the difference in vibrations of all atomic sites between the HT and LT phases induces significant entropy changes which are the main driving force for the transition. Large entropic effects arising primarily from vibrational entropy across a transition are rare in molecular systems since entropy changes normally originate from configurational alterations related to different molecular ordering states. However, such effects have been seen in the open-pore to closed-pore transitions that are found in a small number of metal–organic frameworks.[37,38] Taking advantage of the abundant chemical diversity of HOIPs, the present study reveals a new aspect of their extensive PT landscape and highlights some fundamentally different features of these transitions at the atomic level, especially highlighting the possibility of achieving new desirable properties by manipulating collective modes. Furthermore, considering the fact that many important properties of perovskites are consequences of PTs, the cooperative contributions of all A, B, and X sites for driving PTs in HOIPs can give rise to novel functionalities that conventional perovskites are unable to exhibit. For example, ferroelectric phase transitions driven by vibrational entropy changes offer a new avenue for designing ferroelectric materials and related smart devices beyond the traditional routes. Another example is that the hybrid improper mechanism for creating ferroelectricity endowed by the synergistic involvement of all sites in HOIPs offers much more tunability owing to the presence of organic degree of freedoms not available in perovskite oxides.[39,40] Finally, viewed from a broader perspective, we believe that the subtle interplay between thermodynamic driving mechanisms—balancing entropy,[41] electrostatics, and hydrogen bonding—can stimulate and guide the discovery of new ferroic HOIPs and other hybrid materials.

Acknowledgements

The authors acknowledge the funding support from the National Natural Science Foundation of China (Grant no.

21571072). W.W., G.F., W.L. and P.L. thank the Fundamental Research Funds for the Central Universities, HUST (Grant no. 2017KFXKJC002). W.L. is grateful to Prof. Song Gao for his illuminating suggestions.

Conflict of interest

The authors declare no conflict of interest.

Keywords: ab initio lattice dynamics calculations · hybrid organic–inorganic perovskites · phase transitions · vibrational entropy

How to cite: *Angew. Chem. Int. Ed.* **2018**, *57*, 8932–8936
Angew. Chem. **2018**, *130*, 9070–9074

[1] B. Saparov, D. B. Mitzi, *Chem. Rev.* **2016**, *116*, 4558–4596.
[2] W. Li, Z. Wang, F. Deschler, S. Gao, R. H. Friend, A. K. Cheetham, *Nat. Rev. Mater.* **2017**, *2*, 16099.
[3] W.-J. Xu, Z.-Y. Du, W.-X. Zhang, X.-M. Chen, *CrystEngComm* **2016**, *18*, 7915–7928.
[4] G. Kieslich, A. L. Goodwin, *Mater. Horiz.* **2017**, *4*, 362–366.
[5] W. Zhang, R.-G. Xiong, *Chem. Rev.* **2012**, *112*, 1163–1195.
[6] W.-Y. Zhang, Y.-Y. Tang, P.-F. Li, P.-P. Shi, W.-Q. Liao, D.-W. Fu, H.-Y. Ye, Y. Zhang, R.-G. Xiong, *J. Am. Chem. Soc.* **2017**, *139*, 10897–10902.
[7] C. J. Howard, H. T. Stokes, *Acta Crystallogr. Sect. B* **1998**, *54*, 782–789.
[8] H. T. Stokes, E. H. Kisi, D. M. Hatch, C. J. Howard, *Acta Crystallogr. Sect. B* **2002**, *58*, 934–938.
[9] H. L. B. Boström, J. A. Hill, A. L. Goodwin, *Phys. Chem. Chem. Phys.* **2016**, *18*, 31881–31894.
[10] P.-P. Shi, Y.-Y. Tang, P.-F. Li, W.-Q. Liao, Z.-X. Wang, Q. Ye, R.-G. Xiong, *Chem. Soc. Rev.* **2016**, *45*, 3811–3827.
[11] L. C. Gómez-Aguirre, B. Pato-Doldán, A. Stroppa, L. M. Yang, T. Frauenheim, J. Mira, M. A. Señarís-Rodríguez, *Chem. Eur. J.* **2016**, *22*, 1–9.
[12] Z.-Y. Du, Y.-Z. Sun, S.-L. Chen, B. Huang, Y.-J. Su, T.-T. Xu, W.-X. Zhang, X.-M. Chen, *Chem. Commun.* **2015**, *51*, 15641–15644.
[13] Z.-Y. Du, T.-T. Xu, B. Huang, Y.-J. Su, W. Xue, C.-T. He, W.-X. Zhang, X.-M. Chen, *Angew. Chem. Int. Ed.* **2015**, *54*, 914–918; *Angew. Chem.* **2015**, *127*, 928–932.
[14] P. Jain, N. S. Dalal, B. H. Toby, H. W. Kroto, A. K. Cheetham, *J. Am. Chem. Soc.* **2008**, *130*, 10450–10451.
[15] W. Zhang, Y. Cai, R. G. Xiong, H. Yoshikawa, K. Awaga, *Angew. Chem. Int. Ed.* **2010**, *49*, 6608–6610; *Angew. Chem.* **2010**, *122*, 6758–6760.
[16] J. M. Bermúdez-García, M. Sánchez-Andújar, S. Yáñez-Vilar, S. Castro-García, R. Artiaga, J. López-Beceiro, L. Botana, A. Alegría, M. A. Señarís-Rodríguez, *J. Mater. Chem. C* **2016**, *4*, 4889–4898.
[17] D. B. Mitzi, *Prog. Inorg. Chem.* **1999**, *48*, 1–121.
[18] R. Shang, S. Chen, B.-W. Wang, Z.-M. Wang, S. Gao, *Angew. Chem. Int. Ed.* **2016**, *55*, 2097–2100; *Angew. Chem.* **2016**, *128*, 2137–2140.
[19] J. A. Hill, A. L. Thompson, A. L. Goodwin, *J. Am. Chem. Soc.* **2016**, *138*, 5886–5896.
[20] D.-W. Fu, W. Zhang, H.-L. Cai, Y. Zhang, J.-Z. Ge, R.-G. Xiong, S. D. Huang, T. Nakamura, *Angew. Chem. Int. Ed.* **2011**, *50*, 11947–11951; *Angew. Chem.* **2011**, *123*, 12153–12157.
[21] S. T. Lagerwall, *Ferroelectrics and antiferroelectrics*, Academic Press, New York, **1957**.
[22] M. E. Lines, A. M. Glass, *Principles and applications of ferroelectrics and related materials*, Oxford University Press, Oxford, **1977**.
[23] G. Kieslich, S. Kumagai, K. T. Butler, T. Okamura, C. H. Hendon, S. Sun, M. Yamashita, A. Walsh, A. K. Cheetham, *Chem. Commun.* **2015**, *51*, 15538–15541.
[24] X.-H. Zhao, X.-C. Huang, S.-L. Zhang, D. Shao, H.-Y. Wei, X.-Y. Wang, *J. Am. Chem. Soc.* **2013**, *135*, 16006–16009.
[25] A. M. Glazer, *Acta Crystallogr. Sect. B* **1971**, *28*, 3384–3392.
[26] M. A. Carpenter, *J. Phys. Condens. Matter* **2015**, *27*, 263201.
[27] R. E. McKnight, M. A. Carpenter, T. W. Darling, A. Buckley, P. A. Taylor, *Am. Mineral.* **2007**, *92*, 1665–1672.
[28] W. Li, Z. Zhang, E. G. Bithell, A. S. Batsanov, P. T. Barton, P. J. Saines, P. Jain, C. J. Howard, M. A. Carpenter, A. K. Cheetham, *Acta Mater.* **2013**, *61*, 4928–4938.
[29] R. I. Thomson, P. Jain, A. K. Cheetham, M. A. Carpenter, *Phys. Rev. B* **2012**, *86*, 214304.
[30] A. Stroppa, C. Quarti, F. D. Angelis, S. Picozzi, *J. Phys. Chem. Lett.* **2015**, *6*, 2223–2231.
[31] H. T. Stokes, D. M. Hatch, B. J. Campbell, ISOTROPY, **2007**.
[32] H. T. Stokes, S. Orden, B. J. Campbell, *J. Appl. Crystallogr.* **2016**, *49*, 1849–1853.
[33] K. T. Butler, K. Svane, G. Kieslich, A. K. Cheetham, A. Walsh, *Phys. Rev. B* **2016**, *94*, 180103.
[34] K. T. Butler, A. Walsh, A. K. Cheetham, G. Kieslich, *Chem. Sci.* **2016**, *7*, 6316–6324.
[35] C. C. Stoumpos, C. D. Malliakas, M. G. Kanatzidis, *Inorg. Chem.* **2013**, *52*, 9019–9038.
[36] W. Wang, L.-Q. Yan, J.-Z. Cong, Y.-L. Zhao, F. Wang, S.-P. Shen, T. Zou, D. Zhang, S.-G. Wang, X.-F. Han, Y. Sun, *Sci. Rep.* **2013**, *3*, 2024.
[37] M. T. Wharmby, S. Henke, T. D. Bennett, S. R. Bajpe, I. Schwedler, S. P. Thompson, F. Gozzo, P. Simoncic, C. Mellot-Draznieks, H. Tao, Y. Yue, A. K. Cheetham, *Angew. Chem. Int. Ed.* **2015**, *54*, 6447–6451; *Angew. Chem.* **2015**, *127*, 6547–6551.
[38] A. M. Walker, B. Civalleri, B. Slater, C. Mellot-Draznieks, F. Corà, C. M. Zicovich-Wilson, G. Román-Pérez, J. M. Soler, J. D. Gale, *Angew. Chem. Int. Ed.* **2010**, *49*, 7501–7503; *Angew. Chem.* **2010**, *122*, 7663–7665.
[39] A. Stroppa, P. Barone, P. Jain, J. M. Perez-Mato, S. Picozzi, *Adv. Mater.* **2013**, *25*, 2284–2290.
[40] D. Di Sante, A. Stroppa, P. Jain, S. Picozzi, *J. Am. Chem. Soc.* **2013**, *135*, 18126–18130.
[41] C. Katan, A. D. Mohite, J. Even, *Nat. Mater.* **2018**, *17*, 377.

Manuscript received: March 15, 2018
Accepted manuscript online: May 29, 2018
Version of record online: June 20, 2018

